PERGAMON

International Journal of Solids and Structures 37 (2000) 7003–7027

INTERNATIONAL JOURNAL OF SOLIDS and STRUCTURES

www.elsevier.com/locate/ijsolstr

Computation of kinematic paths and bifurcation points

P. Kumar [1], S. Pellegrino *

Department of Engineering, University of Cambridge, Trumpington Street, Cambridge CB2 1PZ, UK

Received 10 November 1999

Abstract

This article deals with the kinematic simulation of movable structures that go through special configurations of kinematic bifurcation, as they move. A series of algorithms are developed for structures that can be modelled using pin-jointed bars and that admit a single-parameter motion. These algorithms are able to detect and locate any bifurcation points that exist along the path of the structure and, at each bifurcation point, can determine all possible motions of the structure. The theory behind the algorithms is explained, and the analysis of a simple example is discussed in detail. Then, a simplified version of the particular problem that had motivated this work, the simulation of the folding and deployment of a thin membrane structure forming a solar sail, is analysed. For the particular cases that are considered, it is found that the entire process is inextensional, but a detailed study of the simulation results shows that in more general cases, it is likely that stretching or wrinkling will occur.

Keywords: Kinematic bifurcation; Deployable structures; Multibody system

1. Background and introduction

The work described in this article was motivated by difficulties encountered in the kinematic simulation of deployable structures using standard algorithms. It had been found that, as the simulation of the motion of a structure progressed through different configurations, at some points, it became ill conditioned and stopped. When the simulation was re-started, after the configuration of the structure had been perturbed by a small amount, the predicted behaviour appeared to be very sensitive to the particular perturbation that had been applied. It was realised that these difficulties were due to the existence of bifurcation points along the kinematic path followed by the structure. A particular problem that had proved insoluble was the simulation of the folding/unfolding of a thin membrane forming a solar sail, which had been shown to work fine by physical modelling (Guest and Pellegrino, 1992).

Consider, for example, the two-dimensional pin-jointed structure shown in Fig. 1(a). Obviously, bar 2 can be moved horizontally, either to the left or to the right, and downwards by mobilising its single finite amplitude mechanism. Denoting by m the number of independent mechanisms, $m = 1$ here. If bar 2 is moved to the right, the configuration shown in Fig. 1(b) will be obtained and, continuing to mobilise the

* Corresponding author. Tel.: +44-1223-332-721; fax: +44-1223-332-662.
E-mail address: pellegrino@eng.cam.ac.uk (S. Pellegrino).
[1] Present address: Andersen Consulting & Co., 426 World Trade Centre, Barakhamba Lane, New Delhi, India.

0020-7683/00/$ - see front matter
PII: S0020-7683(99)00327-3

Nomenclature

b	number of bars
$\mathbf{C}$	compatibility matrix $(b \times dj)$
$\mathbf{c}_i$	row i of $\mathbf{C}(1 \times dj)$
d	dimension of space (2 or 3)
$\mathbf{d}$	vector of joint displacements (dj)
$\mathbf{d}_i$	nodal displacements of bar i $(2d)$
$\mathbf{e}$	vector of bar extensions (b)
$\mathbf{H}$	equilibrium matrix $(dj \times b)$
j	number of unconstrained joints
ℓ	path length
m	number of independent inextensional mechanisms
$\mathbf{p}$	load vector (dj)
P^i	ith kinematic path
$\mathbf{Q}_j$	coefficient matrix of jth quadratic form $(m \times m)$
$\bar{\mathbf{Q}}_j$	orthonormal form of $\mathbf{Q}_j(m \times m)$
r	rank of equilibrium/compatibility matrix
$\mathbf{R}^P$	point P in configuration space
s	number of states of self-stress
$\mathbf{S}$	second-order compatibility matrix $(2d \times 2d)$
$\mathbf{t}$	vector of bar forces (b)
$\mathbf{u}^i_{r+j}$	jth inextensional mechanism of structure in configuration $\mathbf{R}^i(dj)$
$\mathbf{U}$	matrix of left singular vectors $(dj \times dj)$
$\mathbf{U}_i$	matrix containing rows of $\mathbf{U}_m$ corresponding to bar $i(2d \times m)$
$\mathbf{U}_m$	matrix of inextensional mechanisms $(dj \times m)$
$\mathbf{V}$	matrix of singular values $(dj \times b)$
$\mathbf{W}$	matrix of right singular vectors $(b \times b)$
$\mathbf{W}_s$	matrix of states of self-stress $(b \times s)$
x, y, z	Cartesian coordinates
β_i	ith solution vector (m)
δ	displacement amplitude parameter

mechanism in the same direction, finally the configuration shown in Fig. 1(c) is obtained. In this configuration, two different types of motion are possible, hence $m = 2$. In the first motion, bar 2 remains parallel to the base, Fig. 1(b), whereas in the second motion bar 1 does not move while bars 2 and 3 rotate about joint 1, Fig. 1(d). Note that this choice between two different motions is available only in the particular configuration of Fig. 1(c); once the structure has left this special configuration, its motion is again determined by a single parameter.

All configurations of a movable structure can be represented in a configuration space of suitable dimension. In this example, this space is $\Re^4$ because the positions of joints 1 and 2 can be defined by two cartesian coordinates per joint. A sequence of configuration changes of the type described above defines a *kinematic path* in this configuration space, and the special configuration of Fig. 1(c) corresponds to a point of intersection of two different paths. This point is called a *kinematic bifurcation point*.

Further insight can be gained by analysing the equilibrium matrix for the structure of Fig. 1 (Pellegrino and Calladine, 1986). In the initial configuration, Fig. 1(a), the equilibrium matrix is

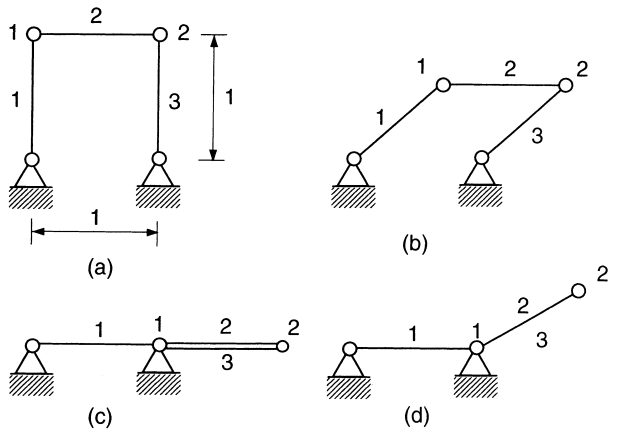

Fig. 1. A three-bar planar structure that has $s = 0, m = 1$ in any ordinary configuration (a, b); (c) kinematic bifurcation with $s = 1$, $m = 2$; (d) one of two possible motions out of bifurcation point.

$$\mathbf{H} = \begin{bmatrix} 0 & -1 & 0 \\ 1 & 0 & 0 \\ 0 & 1 & 0 \\ 0 & 0 & 1 \end{bmatrix}, \tag{1}$$

whose rank is $r = 3$. In the configuration of Fig. 1(c), $\mathbf{R}^C$, the equilibrium matrix is

$$\mathbf{H}' = \begin{bmatrix} 1 & -1 & 0 \\ 0 & 0 & 0 \\ 0 & 1 & 1 \\ 0 & 0 & 0 \end{bmatrix}, \tag{2}$$

whose rank is $r = 2$.

The number of independent inextensional mechanisms of a pin-jointed structure is given by

$$m = 2j - r, \tag{3}$$

where j is the number of unconstrained joints of the structure. The number of independent states of self-stress, i.e. sets of bar forces that are in equilibrium with zero external loads, is

$$s = b - r, \tag{4}$$

where b is the number of bars. According to Eqs. (3) and (4), the structure shown in Fig. 1 has $m = 1$ and $s = 0$ in the initial configuration, but $m = 2$ and $s = 1$ at the bifurcation point, thus showing that the bifurcation points are also special configurations that admit a state of self-stress.

Returning to the configuration shown in Fig. 1(d), let us rotate bars 2 and 3 until they overlap with bar 1. This configuration, $\mathbf{R}^B$, is also a bifurcation point where, again, two different motions are possible, $m = 2$. We can either rotate bars 1 and 2 about joint 2, which now coincides with the left-hand support, or rotate bars 2 and 3 about joint 1, which coincides with the right-hand support. Once one of these two options has been chosen, the structure starts following another single-parameter path.

A topological map of all existing kinematic paths for this structure is shown in Fig. 2. This figure shows that there are three bifurcation points ($\mathbf{R}^B$ and $\mathbf{R}^C$ have been discussed above, while $\mathbf{R}^A$ corresponds to a configuration symmetric to $\mathbf{R}^C$) linked by three kinematic paths. The upper and lower parts of each path are labelled P^i and $P^{i\prime}$. At a bifurcation point, the structure can either continue moving on a path with the same number, or it can switch to a path with a different number.

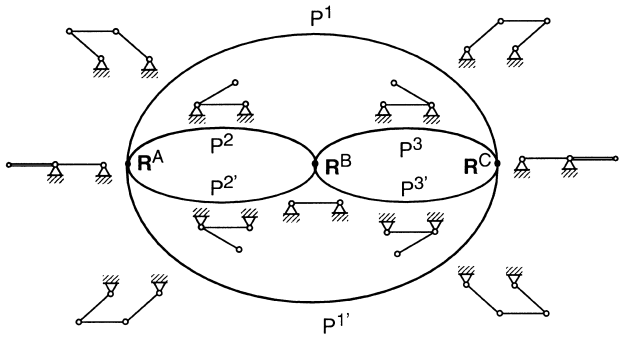

Fig. 2. Topological graph showing all possible kinematic paths of three-bar structure of Fig. 1.

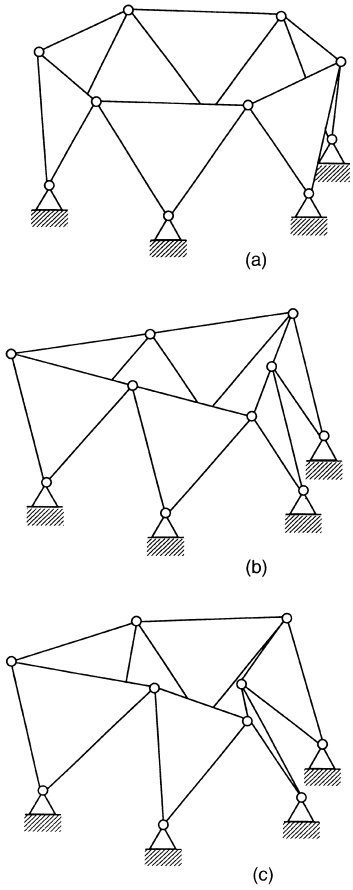

Fig. 3. A hexagonal ring structure with $s = m = 1$ in any ordinary configuration (a, c), but $m = 3$ at the point of bifurcation (b).

The kind of behaviour that is illustrated by the above example occurs in a variety of structures that admit one or more finite-amplitude motions, but in most cases obtaining a complete map like that shown in Fig. 2 is by no means straightforward. A three-dimensional example is the ring structure shown in Fig. 3. It is well-known (e.g. Tarnai, 1980) that in the configuration shown in Fig. 3(a), this structure has a finite mechanism where the joints of the upper hexagon move alternately inwards and outwards so that, although

the six-fold rotational symmetry of the initial configuration is immediately lost, threefold rotational symmetry is maintained. Tarnai (1989) has pointed out that the degree of kinematic indeterminacy increases from $m = 1$ to $m = 3$ when the structure reaches the special configuration shown in Fig. 3(b). At this point, the structure can either continue moving along the same path, thus preserving its threefold rotational symmetry, or it can join a number of alternative paths leading to unsymmetric configurations, e.g. Fig. 3(c).

Kinematic bifurcations are not limited to pin-jointed structures. They have been shown to occur in movable pairs of regular tetrahedra with edges in sliding contact (Tarnai and Makai, 1989), and in many mechanical linkages. Special configurations where the mobility of a linkage transitorily increases, are referred to as *uncertainty configurations* by Hunt (1978). Other authors have referred to such configurations as "cross-over positions", "flattened configurations" or "locking configurations". Some of these terms are, however, only applicable to the case of planar mechanisms. Hunt states that a linkage does not ordinarily encounter an uncertainty configuration unless specially proportioned, we will return to this point at the end of the article, and that "uncertainty configurations need to be systematically studied, and suitable analytical techniques developed to identify them, so that a mechanism designer can recognise them and back away from them into safer regions."

Hunt (1978) makes a distinction between *stationary* and *uncertainty* configurations. At a stationary configuration, one of the joint-freedoms is transitorily inactive. Therefore, even if such a joint were locked, some motion of the other joints would be possible and although theoretically this motion may be only infinitesimal, in practice it may be finite due to the existence of joint clearances. A stationary configuration can be simple or multiple, depending on the number of joint-freedoms that are simultaneously inactive. An uncertainty configuration is, with our terminology, the same as a kinematic bifurcation. Amongst other authors, Sugimoto et al. (1982) have developed a method for determining both stationary and uncertainty configurations of single-loop mechanisms using screw theory. More recently, Litvin et al. (1986) have investigated the singularities in motion occurring in spatial linkages. They fix the driving link and examine the infinitesimal mobility of the remaining links, which is given by the rank of a system matrix. Litvin and Tan (1988) applied this technique to a specific linkage.

This article develops a series of algorithms forming a computational scheme to simulate the continuous motion of a deployable structure that can be modelled using pin-jointed bars, and which admits a single-parameter motion. The scheme is able to detect any bifurcation points that exist along the path of the structure. At each bifurcation point, all possible motions of the structure can be determined, so that a particular one can be selected by the user. The layout of the article is as follows: Section 2 gives a brief outline of the computational scheme. Section 3 presents the theory behind the various algorithms that are used, which are divided into first-order algorithms that stimulate the motion along a uniquely determined path, and second-order algorithms that determine all possible paths out of a kinematic bifurcation point. Two solution techniques are described for the resulting system of quadratic equations, with different levels of accuracy and computational overhead. Section 4 describes the algorithm to converge to a bifurcation point. The algorithms are applied to two simple examples in Section 5, and to the deployment simulation of two small models of solar sail structures, in Section 6. Section 7 concludes the article.

2. Outline of kinematic simulation

The computations that are performed are based on the equilibrium matrix, **H**, of the structure. Alternatively, they could be formulated in terms of the transpose of the equilibrium matrix, i.e. the compatibility matrix. The singular value decomposition (SVD) of **H** is used to identify complete sets of independent inextensional mechanisms, from which any rigid-body mechanisms are removed, and independent states of self-stress.

If the structure is at a bifurcation point, it is necessary to determine which of its mechanisms or their combinations extend into finite motions. Although any linear combination of the set of the inextensional

mechanisms defines, to the first-order, a different kinematic path, only those motions that satisfy a system of second-order compatibility equations are, in fact, potential finite motions. Further, it is possible that some paths actually coincide, and this can be discovered only by actually simulating finite-amplitude motions of the structure.

Once a path out of a point of bifurcation has been selected, the single internal mechanism of the structure is mobilised until the structure reaches the next bifurcation point. Along this single-parameter path, a predictor–corrector algorithm based on the SVD of the equilibrium matrix is implemented, and a special algorithm is developed to detect the existence of a bifurcation ahead of the current configuration, and to stop exactly there. Then, the analysis at the point of bifurcation is repeated.

Fig. 4 shows the path followed by a structure, initially at the bifurcation point $\mathbf{R}^0$. Three different paths can be taken at $\mathbf{R}^0$, and each path has two different directions. Having chosen P^1, a single-parameter motion is simulated until the assembly moves into another point of bifurcation, $\mathbf{R}^n$.

3. Theory

Consider a pin-jointed structure with b bars and j non-foundation joints. The equilibrium matrix $\mathbf{H}$, relating the vector of bar forces, $\mathbf{t}$, to the vector of nodal load components, $\mathbf{p}$, has dj rows, where $d = 2$ or 3 is the dimension of the space in which the structure is being analysed, and b columns

$$\mathbf{Ht} = \mathbf{p}. \tag{5}$$

The compatibility matrix relating the (small) nodal displacement components, $\mathbf{d}$, to the bar extensions, $\mathbf{e}$, is

$$\mathbf{Cd} = \mathbf{e}. \tag{6}$$

It can be shown, e.g. by virtual work that

$$\mathbf{C} = \mathbf{H}^{\mathrm{T}}. \tag{7}$$

3.1. First-order analysis

A general discussion of the links between linear structural mechanics and linear operators, that provides a background to this section, can be found in Besseling (1979). The first step in the computational pro-

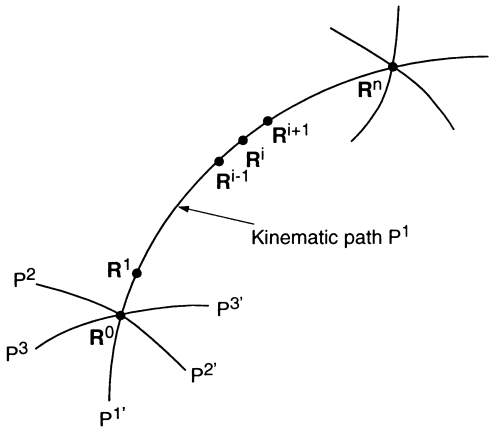

Fig. 4. Kinematic path with bifurcation points at $\mathbf{R}^0$ and $\mathbf{R}^n$.

cedure is the determination of the total number of independent inextensional mechanisms m and the number of states of self-stress s. These parameters can be determined from the rank r of the equilibrium matrix $\mathbf{H}$

$$m = dj - r, \tag{8}$$

$$s = b - r. \tag{9}$$

In non-bifurcation configurations, the structures considered in this article have a single mechanism, $m = 1$, and no states of self-stress, $s = 0$. Hence, from Eqs. (8) and (9)

$$dj - b = 1.$$

The value of r is determined, together with orthogonal sets of m inextensional mechanisms and s states of self-stress, from the SVD of the equilibrium matrix (Golub and van Loan, 1983; Pellegrino, 1993). The SVD of the equilibrium matrix consists of a set of left singular vectors $\mathbf{U} = [\mathbf{u}_1, \ldots, \mathbf{u}_{dj}]$, a set of right singular vectors $\mathbf{W} = [\mathbf{w}_1, \ldots, \mathbf{w}_b]$ and a set of non-zero singular values

$$\mathbf{V} = \left[\begin{array}{c|c} \mathrm{diag}(v_1, \ldots, v_r) & 0 \\ \hline 0 & 0 \end{array}\right]$$

such that

$$\mathbf{H} = \mathbf{U}\mathbf{V}\mathbf{W}^{\mathrm{T}}. \tag{10}$$

The singular vectors, of unit magnitude, can be grouped into the following sub-matrices

$$\begin{aligned} \mathbf{U}_r &= [\mathbf{u}_1, \ldots, \mathbf{u}_r], \quad \mathbf{U}_m = [\mathbf{u}_{r+1}, \ldots, \mathbf{u}_{r+m}], \\ \mathbf{W}_r &= [\mathbf{w}_1, \ldots, \mathbf{w}_r], \quad \mathbf{W}_s = [\mathbf{w}_{r+1}, \ldots, \mathbf{w}_{r+s}]. \end{aligned} \tag{11}$$

Because of the correspondence between equilibrium and compatibility matrices, Eq. (7), the singular vectors have the following physical interpretation:

$\mathbf{U}_r$ – contains modes of extensional deformation
(loads that can be equilibrated by the structure, in its current configuration);
$\mathbf{U}_m$ – contains modes of inextensional deformation, or mechanisms
(loads that cannot be equilibrated);
$\mathbf{W}_r$ – contains sets of kinematically compatible extensions corresponding, through the singular values, to the extensional modes in $\mathbf{U}_r$
(bar forces in equilibrium with the external loads in $\mathbf{U}_r$);
$\mathbf{W}_s$ – contains sets of kinematically incompatible extensions
(states of self-stress).

It follows from the above that a set of bar extention $\mathbf{e}$ is compatible if and only if it satisfies the condition

$$\mathbf{W}_s^{\mathrm{T}}\mathbf{e} = 0. \tag{12}$$

Kinematic bifurcations are associated only with *internal mechanisms*, and hence, if the structure admits any rigid-body mechanisms, they need to be removed from $\mathbf{U}_m$. An algorithm to remove rigid-body

mechanisms from $\mathbf{U}_m$ is described in Pellegrino and Calladine (1986); it will be assumed that $\mathbf{U}_m$ contains only internal mechanisms, m being the number of internal mechanisms.

Two different cases are possible: (i) $m = 1$ with $s = 0$, and hence in the current configuration the structure admits a single-parameter finite motion, or (ii) $m \geqslant 2$ with $s \geqslant 1$, and hence the structure is at a bifurcation point. In other words, because we are considering only assemblies with a single large displacement mechanism, if more than one infinitesimal mechanism is found in some particular configuration, then in that configuration the structure must be at a point of kinematic bifurcation.

Case (i) can be dealt with using the results of the first-order analysis described above, Section 3.2. Case (ii) requires the development of additional theory, Section 3.3, to determine the distinct kinematic paths along which the structure can move out of the bifurcation point. The computation of these kinematic paths requires the use of compatibility equations that include terms of order higher than those included in Eq. (6).

3.2. Predictor–corrector incrementation

Consider a structure with $m = 1$ that is moving along a kinematic path, and assume that the current configuration, $\mathbf{R}^i$, is not a bifurcation point. To find the next configuration of the structure we impose a finite amplitude of its inextensional mechanism $\mathbf{u}^i_{r+1}$ (predictor step) and then carry out a series of iterative corrections (corrector steps) that eliminate any strain in the bars, Fig. 5. The predictor step is

$$\mathbf{R}^{i'} = \mathbf{R}^i + \mathbf{u}^i_{r+1}\delta. \tag{13}$$

The sign of δ controls the direction of motion. Because there is no guarantee that the SVDs of the equilibrium matrices in successive configurations will automatically produce mechanisms with consistent signs, the sign of δ has to be such that the kinematic path continues to be followed in the desired direction. This is ensured by checking the sign of the dot product between the mechanisms in the configurations $i-1$ and i. The sign of δ is reversed if

$$\mathbf{u}^{i-1}_{r+1}\mathbf{u}^i_{r+1} \simeq -1. \tag{14}$$

The maximum value of δ that is allowed (smaller values may be used to increase the number of points on the path) depends upon the region of the kinematic path along which the structure is moving. If the smallest non-zero singular value, v_r, is sufficiently large, the structure is far away from the next bifurcation point, and hence the magnitude of δ is chosen based upon a length parameter, such as the root mean square of all bar lengths. On the contrary, when the structure is converging towards a bifurcation point, it may be necessary to decrease the magnitude of δ, see Section 4.

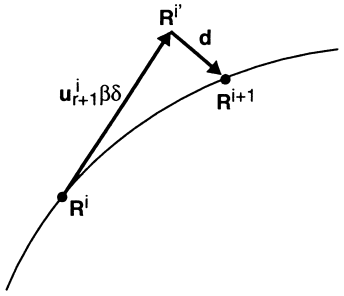

Fig. 5. Predictor–corrector increments along single-parameter path.

In the configuration $\mathbf{R}^{i'}$, the bars of the structure have undergone extensions $\mathbf{e}$ which need to be corrected. Following Besseling et al. (1979) and Pellegrino (1993), the minimal (in a least square sense) correcting displacement $\mathbf{d}$ due to the extensions $-\mathbf{e}$ is computed from

$$\mathbf{d} = -\sum_{i=1}^{r} \frac{\mathbf{w}_i^{\mathrm{T}}\mathbf{e}}{v_i}\mathbf{u}_i. \tag{15}$$

The configuration $\mathbf{R}^{i+1} = \mathbf{R}^{i'} + \mathbf{d}$ is the strain-free configuration nearest to $\mathbf{R}^{i'}$. This corrector step can be repeated a number of times, until a desired convergence accuracy is achieved.

3.3. Second-order compatibility equations

These equations will be derived in two-dimensional space, for compactness, as the extension to the three-dimensional space is trivial. Consider bar i, of length L, between nodes A (X_A, Y_A) and B (X_B, Y_B), Fig. 6. Its length is given by

$$\sqrt{(X_B - X_A)^2 + (Y_B - Y_A)^2} = L. \tag{16}$$

Now, consider a displaced configuration, defined by the nodal displacement components (u_A, v_A) and (u_b, v_B); the new length of the bar is given by

$$\sqrt{[(X_B + u_B) - (X_A + u_A)]^2 + [(Y_B + v_B) - (Y_A + v_A)]^2} = L + e. \tag{17}$$

Squaring both sides

$$[(X_B + u_B) - (X_A + u_A)]^2 + [(Y_B + v_B) - (Y_A + v_A)]^2 = L^2 + e^2 + 2eL. \tag{18}$$

Expanding Eq. (18) and subtracting Eq. (16), we obtain

$$\frac{X_A - X_B}{L}u_A + \frac{Y_A - Y_B}{L}v_A + \frac{X_B - X_A}{L}u_B + \frac{Y_B - Y_A}{L}v_B + \frac{1}{2L}(u_A^2 - 2u_A u_B + u_B^2 + v_A^2 - 2v_A v_B + v_B^2) = e + \frac{e^2}{2L}. \tag{19}$$

The linear part of Eq. (19), i.e. the first four terms on the left-hand side and the first term on the right-hand side, appear already in the linear compatibility equation for the bar, i.e. in the ith equation of the linear system in Eq. 6. The second-order terms on the left-hand-side can be written in matrix form as

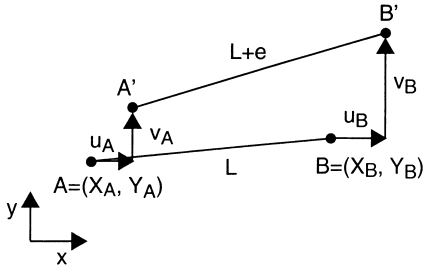

Fig. 6. Original and deformed configurations of bar i.

$$\frac{1}{2L}\begin{bmatrix} u_A & v_A & u_B & v_B \end{bmatrix}\begin{bmatrix} 1 & 0 & -1 & 0 \\ 0 & 1 & 0 & -1 \\ -1 & 0 & 1 & 0 \\ 0 & -1 & 0 & 1 \end{bmatrix}\begin{bmatrix} u_A \\ v_A \\ u_B \\ v_B \end{bmatrix}. \tag{20}$$

Introducing

$$\mathbf{d}_i = \begin{bmatrix} u_A \\ v_A \\ u_B \\ v_B \end{bmatrix}, \quad \mathbf{S} = \begin{bmatrix} 1 & 0 & -1 & 0 \\ 0 & 1 & 0 & -1 \\ -1 & 0 & 1 & 0 \\ 0 & -1 & 0 & 1 \end{bmatrix} \quad \text{and} \quad e_i = e + e^2/2L \tag{21}$$

Eq. (19) becomes

$$\mathbf{c}_i\mathbf{d}_i + \mathbf{d}_i^{\mathrm{T}}\mathbf{S}\mathbf{d}_i = e_i. \tag{22}$$

Here, e_i is a higher-order measure of the extension of bar i which, to the first-order, coincides with the standard measure (current length − initial length). $\mathbf{c}_i$ is the ith row of the compatibility matrix $\mathbf{C}$. For a structure with b bars we can write b equations of this type, one for each bar.

Next, consider the most general motion of nodes A and B that causes no first-order extensions in any bars of the structure. It has the expression

$$\mathbf{d}_i = \mathbf{U}_i\beta, \tag{23}$$

where the vector $\beta = [\beta_1, \ldots, \beta_m]^{\mathrm{T}}$ contains m arbitrary coefficients. $\mathbf{U}_i$ is a matrix with $2d$ rows and m columns, obtained from $\mathbf{U}_m$ by selecting the rows that correspond to bar i. i.e. to nodes A and B.

Substituting Eq. (23) into Eq. (22), we obtain b equations of the type

$$\mathbf{c}_i\mathbf{U}_i\beta + \beta^{\mathrm{T}}\mathbf{U}_i^{\mathrm{T}}\mathbf{S}\mathbf{U}_i\beta = e_i, \quad i = 1, \ldots, b. \tag{24}$$

In Eq. (24), the first term is equal to zero, to the first order, because we are considering a motion that is first-order inextensional. Hence, only the second-order part of the equation needs to be considered

$$\beta^{\mathrm{T}}\mathbf{U}_i^{\mathrm{T}}\mathbf{S}\mathbf{U}_i\beta = e_i^{(2)}. \tag{25}$$

Substituting Eq. (25) into Eq. (12) [2] we obtain a system of s equations, each of the type

$$\sum_{i=1}^{b} t_{i,j}(\beta^{\mathrm{T}}\mathbf{U}_i^{\mathrm{T}}\mathbf{S}\mathbf{U}_i\beta) = 0, \quad j = 1, \ldots, s, \tag{26}$$

where $t_{i,j}$ is the axial force in bar i, for state of self-stress j ($t_{i,j}$ = entry i in $\mathbf{w}_{r+j}$).

Defining

$$\mathbf{Q}_j = \sum_{i=1}^{b} t_{i,j}\mathbf{U}_i^{\mathrm{T}}\mathbf{S}\mathbf{U}_i, \tag{27}$$

the second-order compatibility equations can be written in the form

$$\beta^{\mathrm{T}}\mathbf{Q}_j\beta = 0, \quad j = 1, \ldots, s. \tag{28}$$

This is a system of s quadratic equations, and the kinematic paths out of the point of bifurcation can be obtained by finding the intersections of the corresponding s quadric surfaces. Of the infinite number of first-

[2] This compatibility condition was derived for infinitesimal bar extensions, but it has to be also satisfied by higher-order measures of extension, provided that the configuration of the structure is substantially unchanged.

order inextensional mechanisms $\mathbf{U}_m\beta$, only those particular mechanisms that satisfy the second-order compatibility equations represent potential finite motions.

An alternative derivation of the same second-order compatibility equations can be found in Kuznetsov (1991). The same equations can be obtained also by considering the out-of-balance forces that are induced by imposing small amplitudes of the infinitesimal mechanisms, after applying each state of self-stress onto the structure (Calladine and Pellegrino, 1991).

Before going any further, it is convenient to normalise the quadratic forms in Eq. (28). Computationally, this is done by representing the matrices $\mathbf{Q}_j$ by vectors of length m^2, which are orthogonalised by the Gram–Schmidt technique (Strang, 1980). Each of the resulting unit vectors is then transformed back into a square matrix $\bar{\mathbf{Q}}_j$. So, finally the system of quadratic equation is

$$\beta^{\mathrm{T}}\bar{\mathbf{Q}}_j\beta = 0, \quad \text{for} \quad j = 1, \ldots, s. \tag{29}$$

3.3.1. Solution of second-order compatibility equations

The number of solutions of a system of s algebraic equations of order 2 can be at most 2^s. This follows from *Bezout's Theorem* (Semple and Roth, 1949), which can be stated in the form:

In the projective space S_r, r generic irreducible primals of order $n_1, n_2, \ldots, n_r$, have $n_1 n_2 \ldots n_r$ common points.

Recall that the elements of S_r are points with $r+1$ homogenous coordinates, and a *primal* of order n is the locus of points defined by a polynomial equation of degree n. For s second-order primals, $n_1 = n_2 = \cdots = n_s = 2$ and hence the number of common points is 2^s. Consider the case $s = 3$: the $2^3 = 8$ intersection points of three ellipsoids are shown in Fig. 7(a). Some, or indeed all, of these intersections may be imaginary, Fig. 7(b), or there may be a smaller number of multiple intersections, Fig. 7(c). Finally, there may be *improper intersections* with infinitely many points, Fig. 7(d), in which case Bezout's theorem does not apply.

Both the case of multiple intersections and of improper intersections can be identified by testing the stability of the intersection, i.e. by finding out if the number of intersection points changes for small perturbations of the primals. In practice, because the linear independence of the quadratic forms $\bar{\mathbf{Q}}_j$ does not give any guarantees on the type of intersection, all of the above cases are, in principle, possible.

Two alternative approaches have been implemented to determine the solutions of Eq. (29).

The first approach aims to determine a closed form solution using the method of Gröbner bases (Buchberger, 1985) which is an extension to $r+1$ variables of what one would naturally do for a set of polynomials in only one variable. For such a case, the greatest common divisor of the polynomials can be found and each polynomial can be divided by this divisor to check if the remainder is zero. The method of Gröbner bases extends this idea to multivariate polynomials (Becker and Weispfenning, 1993). Using algebraic rules, a 'Gröbner basis' is constructed for the polynomials. Each polynomial that is to be included in the Gröbner basis is determined by successively reducing the given polynomials and dividing out common factors, and when no further reduction is possible, the polynomial is included in the Gröbner basis. The zeros of the polynomials included in the Gröbner basis determine the roots of the original system of the multivariate algebraic equations.

In recent years, Gröbner bases algorithms have been implemented in symbolic manipulation packages, such as *AXIOM* and *Mathematica*. The function 'solve' in AXIOM determines all possible real roots of a system of the multivariate algebraic equations; however, the runtime of this algorithm grows exponentially with the size of the problem (Buchberger, 1985; Jenks and Sutor, 1992). For our case, as the number of states of self stress s increases, the number of quadratic equations increases correspondingly, and the number of intersections increases exponentially. For example, for $s = 4$ there will be up to $2^4 = 16$ intersections, for $s = 5$ the number of intersections goes up to $2^5 = 32$, and so on. Therefore, although feasible in theory, the method of Gröbner bases is computationally complex and potentially very time consuming.

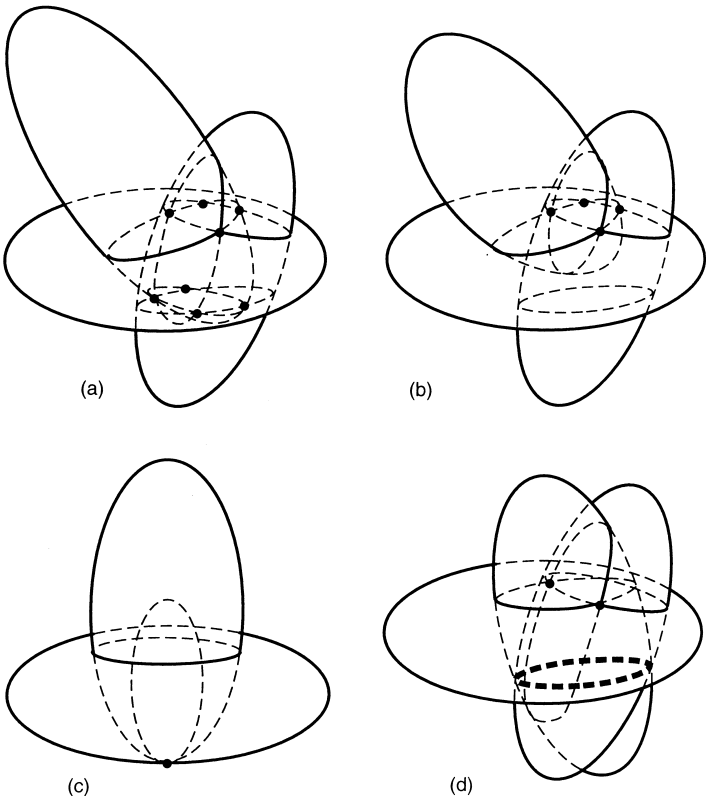

Fig. 7. Intersections of three paraboloids at: (a) eight distinct points; (b) four distinct points; (c) one multiple point; (d) infinitely many points along an ellipse, plus two distinct points.

The computing time for the determination of roots of a system of polynomial equations using AXIOM depends upon two other factors. First, only numeric or symbolic solutions to a system of equations with *exact coefficients* can be found (Jenks and Sutor, 1992). Because the coefficients of Eq. (29), are real numbers, exact coefficients can only be obtained either by truncation into *integers*, or by using a *rational approximation* of the real numbers. In both cases, an error is introduced and the 2^s solutions may no longer be correct. To increase the accuracy, one can increase the number of digits by multiplying each line of Eq. (29) by a suitable scaling factor, before truncating its coefficients, but this slows down the Gröbner factorisation. Runtime is also controlled by the convergence accuracy which is required.

Table 1 compares the solution times required, as s increases, using the methods of integer truncation and rational approximation. For integer truncation, a multiplication factor of 10^3 and a precision value of 10^{-4} were used. For integer truncation, as the multiplication factor is increased, the number of correct roots that are found also increases. However, this is achieved at the expense of additional cpu time. Table 2 shows that finding 13, instead of 12, of the $2^4 = 16$ solutions of the simple space sail model, presented in Section 7 required a seven-fold increase in the cpu time. Note that in all cases AXIOM actually finds 2^s roots, but some are incorrect due to truncation errors. These incorrect roots can be used as the starting points for a numerical, non-linear solver which will find the remaining correct roots. As s increases, the computing times required by AXIOM quickly become impractical; therefore for $s \geqslant 4$, an alternative solution procedure was developed.

Table 1
Solution times using AXIOM (cpu min)

States of self-stress (s)	Computing time		Number of solutions (2^s)	Number of correct solutions
	Integer truncation	Rational approximation		
2	0.2	0.3	4	4
3	0.3	1	8	8
4	21.5	200	16	12

Table 2
Variation of computing time with convergence accuracy, for a problem with $2^4 = 16$ solutions

Multiplication factor	cpu min	Number of correct solutions
10^3	21.5	12
10^4	38.2	12
10^8	153.9	13

The second approach is purely numerical and uses a standard non-linear equation solver. Such algorithms start from an initial starting point and perform a series of iterations to finally converge upon the nearest solution. The key to finding as many different solutions as possible lies in providing well distributed starting points spanning the entire space of first-order mechanisms. As the dimension of the space is $m = s + 1$, whereas there are only s equations, it is necessary to normalise the equations with respect to one variable; this introduces the normalisation condition

$$\|\beta\| = 1. \tag{30}$$

This condition represents the intersection of a hypersphere of unit radius, with the s second-order compatibility equations. For $s = 1$, for example, the space of first-order mechanisms is two-dimensional, and this normalisation is analogous to intersecting a conic with a circle of unit radius. Similarly for $s = 2$, the space of mechanisms is three-dimensional and we look for the intersections of two quadric surfaces with a unit sphere.

By considering well distributed points on this hypersphere and using them as the starting points for the non-linear equation solver "fsolve" available in Matlab (Mathworks, 1997), a number of different solutions are found. Repeated solutions are eliminated by checking the dot product of each new solution with all those found previously. If the dot product is close to 1, the root has already been found. For example, if $n(< 2^s)$ solutions have been determined, then for β_{n+1} the dot products $\beta_i \cdot \beta_{n+1},\ i = 1, \ldots, n$ are computed. If

$$|\beta_i \cdot \beta_{n+1}| \simeq 1 \quad \text{for any } i = 1, \ldots, n, \tag{31}$$

then the root has already been found and the next starting point is considered. Otherwise, β_{n+1} is added to the set of solutions and n is incremented by one.

Depending on how finely the starting points are distributed on the hypersphere, an increasing proportion of the 2^s solutions will be determined. For the same problem with $s = 4$ that was considered above, with 42 initial points, 15 correct solutions were identified in less than 2 cpu min.

3.4. Finite motion paths

Although each solution found in Section 3.3 defines a kinematic path out of the point of kinematic bifurcation, in fact different second-order solutions may correspond to the same kinematic path. To find out, finite-amplitude motions of the structure have to be considered.

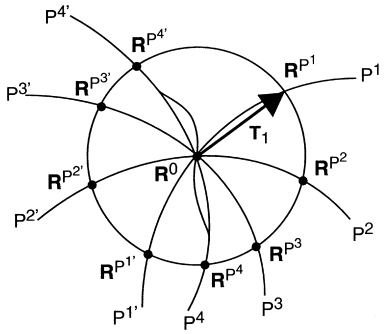

Fig. 8. Identification of distinct finite motions out of a bifurcation point.

Consider a structure at the bifurcation point $\mathbf{R}^0$, Fig. 8, for which a set of solutions of the second-order compatibility equations have been determined with the methods of Section 3.3. Each solution defines a possible finite path for the structure. To test for the existence of the ith finite motion path, we consider the finite-amplitude displacement $\mathbf{R}^0 + \mathbf{U}_m\beta_i\delta$ and then iterate, as explained in Section 3.2, to eliminate any strain in the bars. The corrector step is repeated a number of times, until the desired convergence accuracy is achieved. If the solution does not converge after a specified number of steps, it is deemed that no finite motion path exists in the neighbourhood of the ith solution of Eq. (29).

For each path that is identified, the structure is allowed to move a distance ℓ, measured along the path, using the predictor–corrector algorithm of Section 3.2. The configurations $\mathbf{R}^{Pi}$, all at a distance ℓ from the point of bifurcation $\mathbf{R}^0$, are then compared. Let

$$\mathbf{T}_i = \mathbf{R}^{Pi} - \mathbf{R}^0. \tag{32}$$

To check the path i is different from the previous $i-1$ paths, the dot products of the displacement vectors are computed. If

$$\frac{|\mathbf{T}_i \cdot \mathbf{T}_k|}{\|\mathbf{T}_i\|\|\mathbf{T}_k\|} \simeq 1 \quad \text{for any } j = 1, \ldots, (i-1), \tag{33}$$

then path i has already been identified.

4. Convergence to a bifurcation point

Consider a structure that is moving along a kinematic path, by a series of predictor–corrector steps with a constant step size δ (Section 3.2). As the next bifurcation point is approached, the lowest non-zero singular value v_r starts decreasing. The kinematic simulation has to switch to a different algorithm, which is capable of predicting and stopping exactly at the point of bifurcation, where a new higher-order analysis will be carried out.

Before switching to the algorithm described in this section, two conditions need to be satisfied. First, v_r must be less than a certain threshold value ϵ, indicating that the assembly is getting close to a bifurcation point. Second, v_r should be decreasing in successive steps, i.e. $v_r^{n+1} - v_r^n < 0$.

As the bifurcation point is approached, a number of problems arise. First, there is the danger of numerical ill-conditioning. Second, at the bifurcation point itself it is easy to swap paths, as a number of paths go through this point. Finally, it is possible to jump to the other side of the bifurcation without realising that this had happened.

Consider an assembly in configuration $\mathbf{R}^{n-1}$ approaching a bifurcation point $\mathbf{R}^n$, as shown in Fig. 9. To avoid the problems listed above, it is best to predict the single-step displacement to be imparted to the assembly so that it can be moved directly to $\mathbf{R}^n$. In general, the variation of the smallest singular value near a bifurcation point should be of second- or higher-order. This is because each singular value relates a bar extension vector to a corresponding displacement vector (Pellegrino, 1993). Sampling v_r at the three last configurations, $\mathbf{R}^{n-3}, \mathbf{R}^{n-2}, \mathbf{R}^{n-1}$, a second-order Lagrangian polynomial in ℓ is fitted through these points

$$v_r = a\ell^2 + b\ell + c. \tag{34}$$

The intersection between this polynomial and the axis $v_r = 0$ can be calculated. Depending upon the sign of the coefficient a, two cases are possible. If $a < 0$, Fig. 9(a), the quadratic equation

$$a\ell^2 + b\ell + c = 0 \tag{35}$$

can be solved and, of the two solutions, the one closest to ℓ_{n-1} is chosen.

If $a > 0$, Fig. 9(b), the curve should be tangent to the axis $v_r = 0$, but numerical round-off leads either to the situation in Fig. 10(a), where there is no real solution, or Fig. 10(b), where the quadratic equation admits two solutions. In the former case, ℓ_n is defined from the minimum of the polynomial, in the latter case it is taken to be the solution closest to l_{n-1}.

Having predicted the configuration where v_r is expected to be zero, the amplitude parameter for the step that converges to the bifurcation point is calculated from

$$\delta = \ell_n - \ell_{n-1}. \tag{36}$$

In some cases, it has been observed that the variation of the lowest non-zero singular value near a bifurcation point is linear, rather than quadratic. The reason for this is unclear at present but, as Eq. (34) contains a linear term, it works well in all cases.

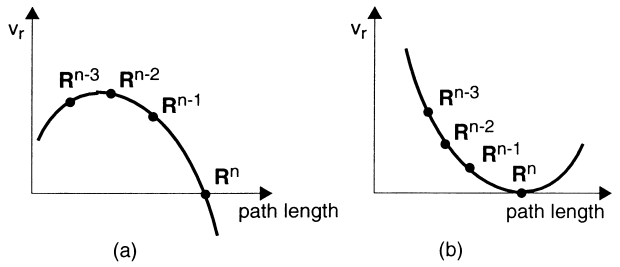

Fig. 9. Variation of lowest non-zero singular value near a bifurcation point.

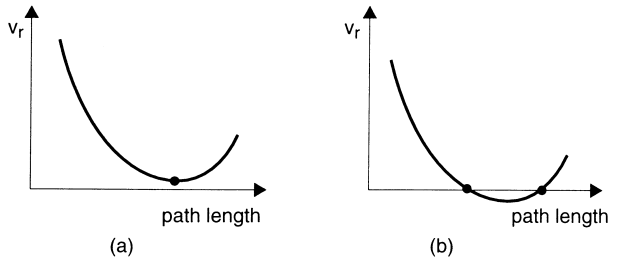

Fig. 10. Effects of numerical errors on lowest non-zero singular value, near a bifurcation point.

Having predicted the displacement amplitude necessary to move the assembly into the point of bifurcation, a forward calculation is performed. Using the value of δ from Eq. (36), the single mechanism in the configuration $\mathbf{R}^{n-1}$ is mobilised and the corresponding strain-free configuration is computed with the standard predictor–corrector algorithm. If in the new configuration $v_r = 0$, then the bifurcation has been found. Otherwise, the following two checks are carried out. First, to ensure that the assembly has not switched paths, it is checked that the inextensional mechanisms in the configuration $\mathbf{R}^{n-1}$ and in the new configuration are approximately identical, hence

$$|\mathbf{u}_{r+1}^{n}\mathbf{u}_{r+1}^{n-1}| \simeq 1. \tag{37}$$

Second, to check that the assembly has yet to reach the bifurcation point a further, small displacement is imparted. If the smallest non-zero singular value is found to increase, it means that the assembly has already crossed the bifurcation point. If both checks are satisfied, the structure is moved from configuration $\mathbf{R}^{n-1}$ to $\mathbf{R}^{n}$. If either check is not satisfied, δ is decreased and the forward calculation is repeated. This iteration is repeated until v_r becomes smaller than a specified tolerance.

5. A simple example

Consider the three-bar structure of Fig. 1, which was already discussed in Section 1. The equilibrium matrix for the structure at the bifurcation point $\mathbf{R}^{C}$, Fig. 1(c), is given in Eq. (2) and its SVD is

$$\mathbf{H}' = \left[\begin{array}{cc|cc} 0.7071 & 0.7071 & 0 & 0 \\ 0 & 0 & -1 & 0 \\ -0.7071 & 0.7071 & 0 & 0 \\ 0 & 0 & 0 & 1 \end{array}\right] \left[\begin{array}{ccc} 1.7321 & 0 & 0 \\ 0 & 1 & 0 \\ 0 & 0 & 0 \\ \hline 0 & 0 & 0 \end{array}\right] \left[\begin{array}{ccc} 0.4082 & -0.8165 & -0.4082 \\ 0.7071 & 0 & 0.7071 \\ \hline 0.5774 & 0.5774 & -0.5774 \end{array}\right]. \tag{38}$$

Hence, the rank of $\mathbf{H}'$ is $r = 2$ and the matrices containing the $m = 2$ mechanisms and $s = 1$ states of self-stress are

$$\mathbf{U}_m = \begin{bmatrix} 0 & 0 \\ -1 & 0 \\ 0 & 0 \\ 0 & 1 \end{bmatrix}, \quad \mathbf{W}_s = \begin{bmatrix} 0.5774 \\ 0.5774 \\ -0.5774 \end{bmatrix}. \tag{39}$$

The coefficient matrix of the second-order compatibility equation is computed from Eq. (27), as follows:

$$\mathbf{Q}_1 = 0.5774 \begin{bmatrix} 0 & -1 \\ 0 & 0 \end{bmatrix} \begin{bmatrix} 1 & 0 \\ 0 & 1 \end{bmatrix} \begin{bmatrix} 0 & 0 \\ -1 & 0 \end{bmatrix} + 0.5774 \begin{bmatrix} 0 & -1 & 0 & 0 \\ 0 & 0 & 0 & 1 \end{bmatrix} \begin{bmatrix} 1 & 0 & -1 & 0 \\ 0 & 1 & 0 & -1 \\ -1 & 0 & 1 & 0 \\ 0 & -1 & 0 & 1 \end{bmatrix} \begin{bmatrix} 0 & 0 \\ -1 & 0 \\ 0 & 0 \\ 0 & 1 \end{bmatrix}$$
$$- 0.5774 \begin{bmatrix} 0 & 0 \\ 0 & 1 \end{bmatrix} \begin{bmatrix} 1 & 0 \\ 0 & 1 \end{bmatrix} \begin{bmatrix} 0 & 0 \\ 0 & 1 \end{bmatrix}. \tag{40}$$

This gives

$$\mathbf{Q}_1 = \begin{bmatrix} 1.1547 & 0.5774 \\ 0.5774 & 0 \end{bmatrix} \tag{41}$$

and, thus, the second-order compatibility equation is

$$[\beta_1\beta_2]\begin{bmatrix} 1.1547 & 0.5774 \\ 0.5774 & 0 \end{bmatrix}\begin{bmatrix} \beta_1 \\ \beta_2 \end{bmatrix} = 0, \tag{42}$$

which can be simplified to

$$\beta_1^2 + \beta_1\beta_2 = 0. \tag{43}$$

Including the normalisation condition, Eq. (30), we obtain the following system of quadratic equations

$$\begin{cases} \beta_1^2 + \beta_1\beta_2 = 0, \\ \beta_1^2 + \beta_2^2 = 1, \end{cases} \tag{44}$$

whose solutions are $\beta_1 = [-1\ 1]^{\mathrm{T}}$ and $\beta_2 = [0\ 1]^{\mathrm{T}}$. These two solutions correspond to two distinct kinematic paths out of $\mathbf{R}^C$, shown in Fig. 1(b) and (d).

We choose path P^1, corresponding to β_1, and follow the motion of the structure, which has a single mechanism, until it approaches the next bifurcation point, $\mathbf{R}^A$. Convergence to this bifurcation point was achieved in a single step; the lowest non-zero singular value in the penultimate step was $v_r = 0.0052$, at this point an amplitude parameter $\delta = 0.0091$ was computed with the method of Section 4, and in the following step $v_r = 7.14 \times 10^{-7}$. Because this number is smaller than the required tolerance (10^{-6}), the structure was considered to have converged to $\mathbf{R}^A$. Hence, a new analysis of the available paths was carried out.

Fig. 11 shows the variation of the lowest non-zero singular value with path length for a complete kinematic simulation starting in configuration $\mathbf{R}^A$, going to $\mathbf{R}^C$ through path P^1, then to $\mathbf{R}^B$ through path P^3, and then back to $\mathbf{R}^A$ through path P^2.

6. Folding and deployment of solar sails

An important motivation for developing the algorithms presented in this article was being able to simulate the folding and deployment of a thin membrane structure that had been proposed by Temple and Oswald (Cambridge Consultants, 1989) for a solar powered spacecraft that would go to Mars. The original

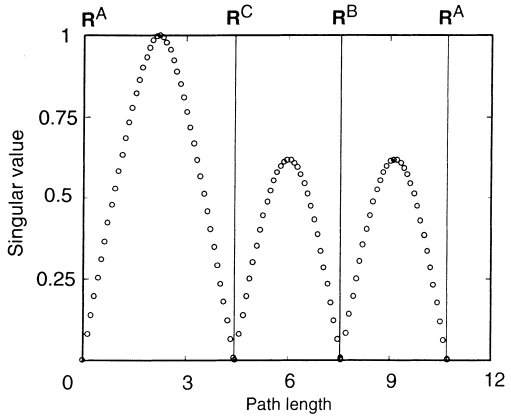

Fig. 11. Variation of lowest non-zero singular value for kinematic simulation along paths P^1, P^3 and P^2, of structure in Fig 1.

proposal envisaged a circular membrane with a diameter of 276 m that, during launch, would be wrapped around a spacecraft with a diameter of 4 m.

Guest and Pellegrino (1992) analysed the folding pattern that is required to wrap such a membrane around a central hub. In the simplest case, Fig. 12(c), this consists of an odd number of near-radial folds that crease the membrane alternately up, *valley folds*, and down, *crest folds*, intersected by sets of parallel folds. The crest and valley folds originate at the corners of a straight-sided polygon that forms the hub.

To make small physical models of this structure, it is fine to assume that the membrane has zero thickness, in which case the crest and the valley folds are straight. However, in larger models, one has to account for the gradual increase in the effective size of the hub as the membrane is wrapped around it.

These fold patterns are worked out by considering only the fully folded and fully deployed configurations. Hence, they do not guarantee that the folding process itself will not require either stretching of the membrane, or changing the shape of the fold lines. The only way of finding out if small effects of this kind play a role in this type of folding is to carry out a kinematic simulation of the folding/deployment process.

Thus, the three main questions to be answered by the simulation are

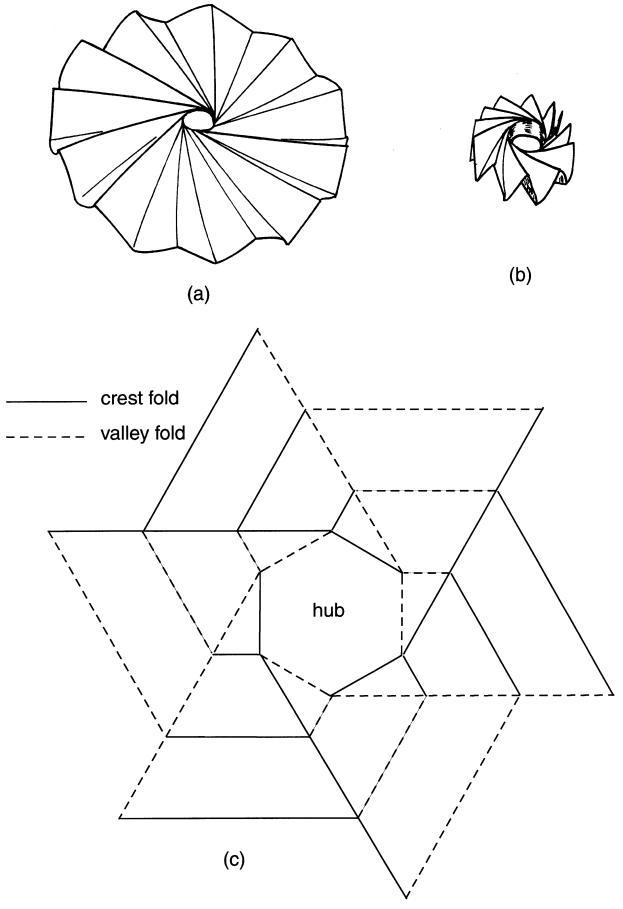

Fig. 12. Wrapping of the thin membrane around a central hub: (a) deployed and (b) wrapped configurations; (c) folding pattern with six near-radial folds.

- Does there exist a continuous, strain-free motion that takes the assembly from the open to the folded configuration?
- Is there a possibility that the membrane might deploy/retract into an unexpected configuration, due to the existence of bifurcation points along its path?
- Does the hub remain planar during this motion?

To answer these questions, the membrane will be assumed to be of zero thickness, and modelled as a pin-jointed bar assembly consisting of bars placed along the fold lines of the membrane. An additional pin-jointed bar is placed along a diagonal of each trapezium bounded by successive parallel folds.

6.1. Square hub

Here, we analyse a solar sail of the smallest possible size and with the smallest possible number of crest and valley folds, i.e. four in total. Its pin-jointed model is shown in Fig. 13. This assembly has $b = 16$ bars and $j = 6$ non-foundation joints. Two joints, 1 and 3, are fully constrained. In a general configuration, this structure has two finite inextensional mechanisms, a rigid-body rotation about the axis 1–3, and an internal mechanism.

To simulate the folding process, the equilibrium matrix of the pin-jointed assembly was set up in the fully deployed, i.e. flat, configuration. The SVD of the equilibrium matrix determines six independent mechanisms and, after elimination of rigid-body mechanism, a set of internal mechanisms $\mathbf{U}_m$ was obtained. A set of independent states of self-stress $\mathbf{W}_s$ was also obtained. As in this configuration, the number of mechanisms is greater than one, the structure is at a bifurcation point, and hence the higher-order analysis of Sections 3.3 and 3.4 was carried out. The $s = 4$ second-order compatibility equations in the $m = 5$ variables $\beta = [\beta_1 \dots \beta_5]$ are

$$\beta^{\mathrm{T}}\mathbf{Q}_i\beta = 0, \quad \text{for } i = 1 \dots 4, \tag{45}$$

where

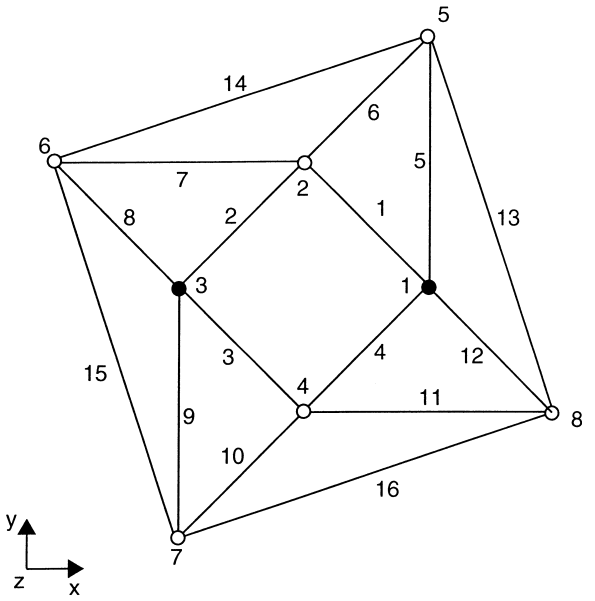

Fig. 13. Pin-jointed model of smallest possible solar sail.

$$\mathbf{Q}_1 = \begin{bmatrix} 407 & 361 & 340 & 92 & -28 \\ 361 & -31 & 302 & -12 & -22 \\ 340 & 302 & 321 & -52 & 4 \\ 92 & -12 & -52 & -156 & 56 \\ -28 & -22 & 4 & 56 & -32 \end{bmatrix},$$

$$\mathbf{Q}_2 = \begin{bmatrix} -258 & 320 & -97 & -129 & 32 \\ 320 & -716 & 18 & 186 & 20 \\ -97 & 18 & -22 & 74 & 56 \\ -129 & 186 & 74 & 251 & -70 \\ 32 & 20 & 56 & -70 & 9 \end{bmatrix},$$

$$\mathbf{Q}_3 = \begin{bmatrix} 134 & -4 & 209 & -166 & 215 \\ -4 & 350 & -66 & 197 & 152 \\ 209 & -66 & 102 & 266 & 74 \\ -166 & 197 & 266 & 513 & -162 \\ 215 & 152 & 74 & -162 & -113 \end{bmatrix},$$

$$\mathbf{Q}_4 = \begin{bmatrix} 52 & -1 & -83 & 4 & -342 \\ -1 & 49 & -59 & -151 & -272 \\ -83 & -59 & 337 & 218 & 311 \\ 4 & -151 & 218 & 209 & -73 \\ -342 & -272 & 311 & -73 & 302 \end{bmatrix}.$$

All entries in the above matrices have been multiplied by 10^3 and then rounded off to the nearest integer. Eq. (45) is subject to the normalisation condition

$$\beta_1^2 + \beta_2^2 + \beta_3^2 + \beta_4^2 + \beta_5^2 = 1. \tag{46}$$

According to Bezout's theorem, $2^4 = 16$ solutions can be expected and, as mentioned in Section 3.3.1, the computing time required to find them by the method of Gröbner bases would be very long. Hence, the root scanning procedure was used and 15 solutions were found in less than two cpu min. Fig. 14 shows the configurations that were obtained by simulating the motion of the structure along these 15 paths. All of these configurations are at a distance $\ell = 1.75$ from the flat configuration. Note that a number of kinematic paths are related by symmetry considerations, as the assembly has four-fold cyclic symmetry and the folding pattern has two-fold symmetry. For example, path 8 can be obtained by rotating path 6, through 180° about the z-axis.

Path 12 corresponds to the path that takes the sail into its fully folded configuration. Nodes 2 and 4 move down (into the paper), whereas nodes 5 and 7 move up (out of the paper). In fact, there is a second path that also takes the sail into its fully folded configuration, corresponding to the 16th solution, which was not identified by the root scanning procedure. This alternative path requires nodes 2 and 4 to move up while nodes 5 and 7 move down. In both cases, two hub nodes have to move out of plane. Thus, depending upon the motion of the hub, up or down, two equivalent kinematic paths leading to the same compact folded pattern exist.

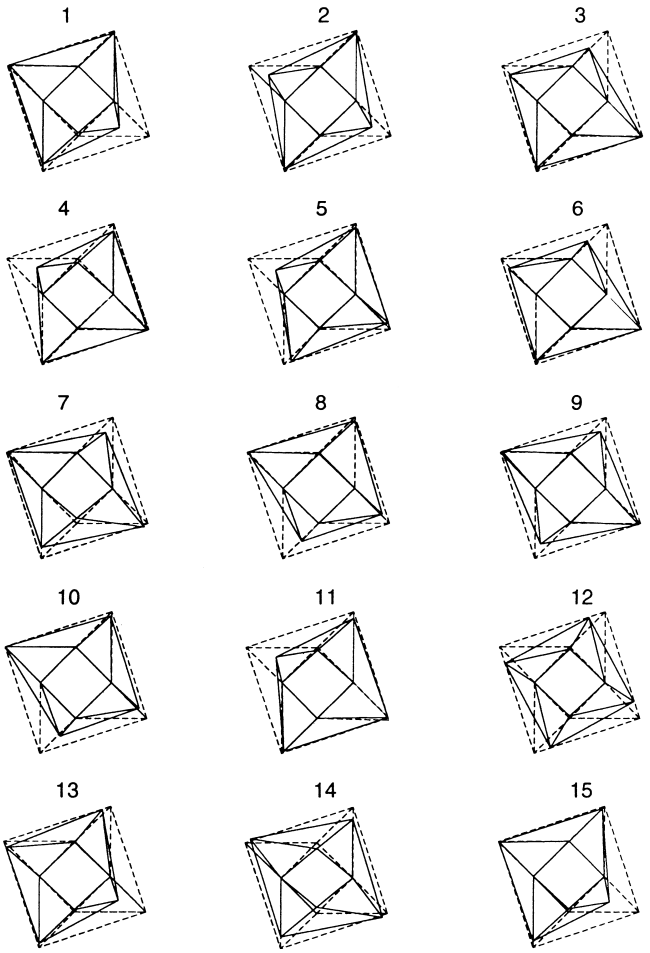

Fig. 14. Projection onto x, y plane of 15 of $2^4 = 16$ motions out of fully deployed configuration, of solar sail with a square hub.

6.2. Hexagonal hub

We will now consider the folding of a pin-jointed structure that consists of two loops of triangles that wrap around a six-sided hub, Fig. 15. This (slightly) more realistic model of the solar sail will allow us to give complete answers to the three questions that were posed at the beginning of this section.

Three of the hub nodes, 2, 4 and 6, are fully constrained. The other nodes are connected by bars to node 1, which is allowed to move only in the z-direction, to maintain the hexagonal shape of the hub. The equilibrium matrix of this assembly has size 46×45. In a general configuration, the assembly has only one finite internal mechanism, but in the fully deployed, flat configuration $\mathbf{R}^A$ in which we started our simulation there are $m = 16$ independent infinitesimal mechanisms and $s = 15$ independent states of self-stress.

After a laborious analysis of this bifurcation point, with its potential 2^{15} paths, the correct kinematic path was picked up, thus starting the motion illustrated in Fig. 16. Fig. 16(c) shows a partially folded configuration, where nodes 8–13 lie directly above or below the hub nodes. This configuration corresponds to the bifurcation point $\mathbf{R}^B$, which our algorithm took 35 steps to converge to. Although in this configuration the hub is planar, it had distorted out-of-plane during the motion from $\mathbf{R}^A$ to $\mathbf{R}^B$. At $\mathbf{R}^B$, there are

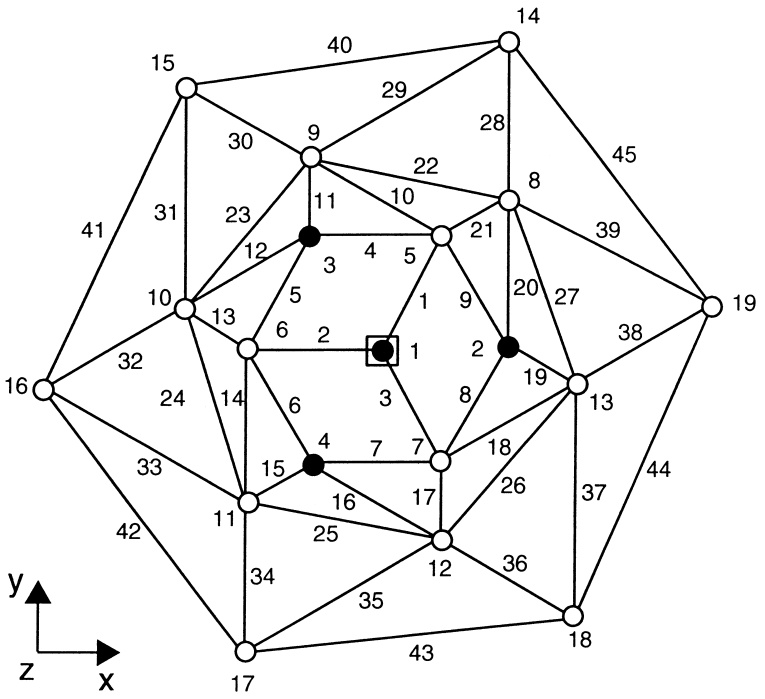

Fig. 15. Pin-jointed model of small solar sail with six near-radial folds and hexagonal hub. cf. Fig 12(c).

$m = 4$ infinitesimal mechanisms and $s = 3$ states of self-stress and, having computed $2^3 = 8$ distinct finite paths, it was found that there are two axisymmetric motions both of which lead to the correct folded configuration. These two solutions correspond to node 1 moving up or down.

As the assembly approached the fully folded configuration $\mathbf{R}^C$, three non-zero singular values started approaching zero. The configuration $\mathbf{R}^C$, shown in Fig. 16(e), is also a bifurcation point, which took 26 steps to converge to. In this configuration, the central hub is again planar.

Next, the structure was deployed back to the original configuration $\mathbf{R}^A$. The deployment simulation began with an analysis of bifurcation point $\mathbf{R}^C$, where an axisymmetric deployment path was chosen. During deployment, the assembly passed through the bifurcation point $\mathbf{R}^B$ and, finally, as it approached the fully open configuration, 15 singular values started approaching zero. Convergence to the bifurcation point $\mathbf{R}^A$ required 149 simulation steps.

The variation of the 15 singular values that were zero at the start of the simulation described above are plotted in Fig. 17 for the entire kinematic simulation. One singular value is always zero, corresponding to the single internal mechanism. Due to the cyclic symmetry of the assembly, some of the singular values coincide and therefore the number of distinct curves that are visible on the plot is actually less than 15.

Note that the plot in Fig. 17 is symmetric about the centre line, as the same path was followed both during folding and deployment. In fact, it is possible to change path at the first bifurcation and follow an alternative path. This would also produce the correct folding pattern, but the variation of the singular values would no longer be symmetric.

Also note that the number of steps taken to converge to successive bifurcation points increased during the course of the simulation. Thus, it took 35, 26, 58 and 149 steps to converge to the bifurcation points $\mathbf{R}^B, \mathbf{R}^C, \mathbf{R}^B$ and $\mathbf{R}^A$, respectively. It appears that there is a link between the rank deficiency of the equilibrium matrix, i.e. the number of singular values that are approaching zero, and the number of iteration steps

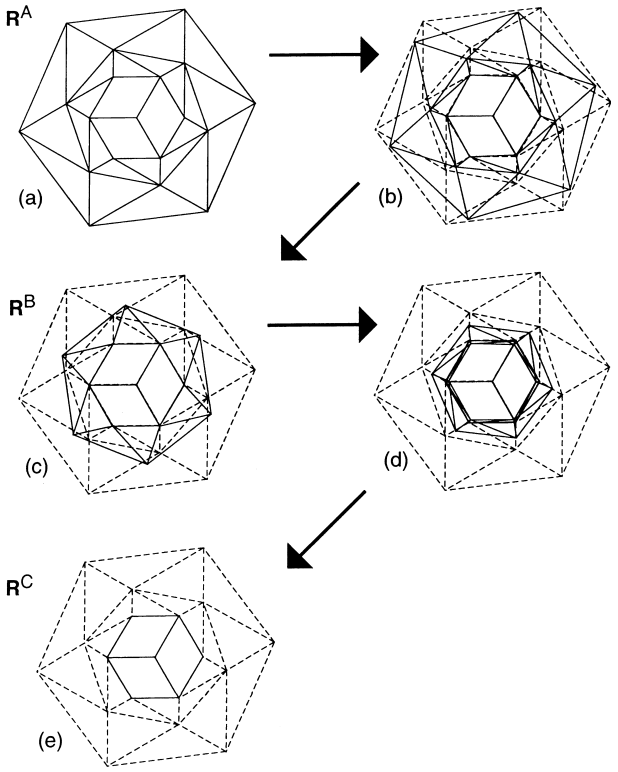

Fig. 16. Projection onto x, y plane of folding simulation of structure in Fig. 15.

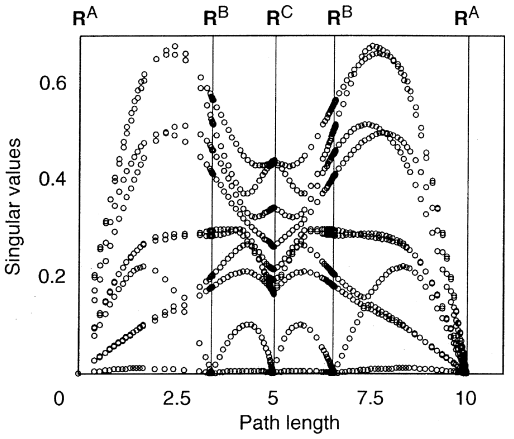

Fig. 17. Variation of 15 lowest non-zero singular values during folding and deployment of solar sail model of Fig. 15.

required for convergence. However, the build up of numerical errors and inaccuracies may also be a significant effect, as convergence to the same configuration, $\mathbf{R}^B$, required 35 steps the first time and 58 the second time.

6.3. Conclusions

The kinematic simulations described in Sections 6.1 and 6.2 suggest that the deployment/folding behaviour of a theoretical membrane of zero thickness and with straight folds is *strictly inextensional*, provided that the hub is allowed to distort out of plane. It has been shown that the deployment process is radially sequential, i.e. a complete loop of triangles has to unwrap completely before the next loop starts unwrapping, and there is a kinematic bifurcation every time a loop completes its unwrapping.

It should be noted that in the simulation, the bars and joints of the pin-jointed model of the solar sail were allowed to pass through each other, although this never happened. It should also be noted that the part of the membrane that is already wrapped around the hub does not remain stationary, but moves by a small amount. This is evident in Fig. 16(d), as a smaller hexagon inside the hub is evidence of the fact that the projections of joints 8–13 have moved beyond the hub joints. So, it can be concluded that, although in the particular simulations that we have carried out there was no physically unacceptable interference between different parts of the membrane, it is likely that there would be interference if one considered a larger solar sail, whose folding pattern consists of several loops of triangles. Of course, the effect of modelling the thickness of the membrane would also need to be considered in this case.

7. Discussion

This article has introduced a series of kinematic simulation techniques for movable structures that can be modelled as pin-jointed assemblies, and which go through kinematic bifurcation points as they move. These techniques have been shown to be a useful tool for the analysis of solar sail-type deployable structures. Further applications are available in Kumar (1996).

We have considered only the case of structures with a single mechanism and no states of self-stress in an ordinary configuration, and which have $s \geqslant 1$ and $m \geqslant 2$ only at bifurcation points. This is the case that is of greatest practical interest for deployable structures, where it is generally required that $m = 1$ to avoid uncertain behaviour during deployment. The analysis of more general types of structures should be a straightforward extension of the algorithms that have been presented here. The only practical difficulty will be in choosing a particular type of motion out of the infinitely many that are possible in any ordinary configuration.

Much more challenging will be going beyond pin-jointed structures, to link our present approach to mechanical linkages with different types of joints. The existence of kinematic bifurcations in deployable structures that cannot be modelled as pin-jointed has already been shown, and it would be interesting to explore the possibility of using higher-order compatibility conditions in that context.

Finally, it should be noted that kinematic bifurcations arise due to a number of bars in an assembly being of equal length, or the sum of the lengths of certain bars being equal to the length of an another bar, etc. It is possible to avoid that a number of kinematic paths converge at the same point by deliberately introducing some imperfections in the structure. In other words, by changing some of the bar lengths the kinematic paths can be separated out, thereby reducing the possibility of the assembly moving along an incorrect kinematic path. Although it is likely that this will always happen in practice, due to manufacturing inaccuracies, it would be useful to carry out systematic studies of which particular types of imperfections should be "designed into the structure" to avoid anomalous behaviour at bifurcation points.

Acknowledgements

We are grateful to Prof. R. Connelly for helpful discussions, and for pointing out to us the usefulness of Bezout's theorem in the present study. Helpful comments by two reviewers are acknowledged. P. Kumar gratefully acknowledges financial support from the Cambridge Commonwealth Trust and the Nehru Trust.

References

Becker, T., Weispfenning, V., 1993. Gröbner Bases: A Computational Approach to Commutative Algebra. Springer, New York.
Besseling, J.F., 1979. Finite element methods. In: Besseling J.F., van der Heijden, A.M.A. (Eds.), Trends in Solid Mechanics 1979. Delft University Press, Delft.
Besseling, J.F., Ernst, L.J., Van der Werff, K., de Koning, A.U., Riks, E., 1979. Geometrical and physical non-linearities. Some developments in the Netherlands. Computer Methods in Applied Mechanics and Engineering 17/18, 131–157.
Buchberger, B., 1985. Gröbner bases: an algorithmic method in polynomial ideal theory. In: Bose, N.K. (Ed.), Multidimensional Systems Theory: Papers, Directions and Open Problems in Multidimensional Systems. Reidel, Dordrecht.
Calladine, C.R., Pellegrino, S., 1991. First-order infinitesimal mechanisms. International Journal of Solids and Structures 27, 505–515.
Cambridge Consultants, 1989. Design Study for a Mars Sailcraft, Q7844/JPA/Issue 1, Cambridge Consultants Ltd.
Golub, G.H., van Loan, C.F., 1983. Matrix Computations. North Oxford Academic Publishing, Oxford.
Guest, S.D., Pellegrino. S., 1992. Inextensional wrapping of flat membranes. In: Motro, R., Wester, T. (Eds.), Proceedings of The First International Seminar on Structural Morphology, LMGC, Universite Montpellier II, Montpellier, pp. 203–215.
Hunt, K.H., 1978. Kinematic Geometry of Mechanisms. Clarendon Press, Oxford.
Jenks, R.D., Sutor, R.S., 1992. AXIOM The Scientific Computation System. The Numerical Algorithms Group. Springer, New York.
Kuznetsov, E.N., 1991. Underconstrained Structural Systems. Springer, New York.
Kumar, P., 1996. Kinematic Bifurcations and Deployment Simulation of Foldable Space Structures. Ph.D. Thesis, University of Cambridge.
Litvin, F.L., Fanghella, P., Tan, J., Zhang, Y., 1986. Singularities in motion and displacement functions of spatial linkages. ASME Journal of Mechanisms, Transmissions, and Automation in Design 108, 516–523.
Litvin, F.L., Tan, J., 1988. Singularities in motion and displacement functions for the RCRCR linkage. ASME Journal of Mechanisms, Transmissions, and Automation in Design 110, 373–377.
Mathworks, 1997. Matlab Version 5: User's Guide. The Math Works, Natick, MA.
Pellegrino, S., Calladine, C.R., 1986. Matrix analysis of statically and kinematically indeterminate frameworks. International Journal of Solids and Structure 22, 409–428.
Pellegrino, S., 1993. Structural computations with the SVD of the equilibrium matrix. International Journal of Solids and Structure 30, 3025–3035.
Semple, J.G., Roth, L., 1949. Introduction to Algebraic Geometry. Clarendon Press, Oxford.
Strang, G., 1980. Linear Algebra and its Applications, Second Ed. Academic Press, New York.
Sugimoto, K., Duffy, J., Hunt, K.H., 1982. Special configurations of spatial mechanisms and robot arms. Mechanism and Machine Theory 17 (2), 119–132.
Tarnai, T., 1980. Simultaneous static and kinematic indeterminacy of space trusses with cyclic symmetry. International Journal of Solids and Structure 16, 347–359.
Tarnai, T., 1989. Finite mechanisms and the timber octagon of Ely Cathedral. Structural Topology 14, 9–20.
Tarnai, T., Makai, E., 1989. A movable pair of tetrahedra. Proceedings of Royal Society London, Part A 423, 419–442.